2018-02-08

Effect of shear stress on distortional buckling of CFS beams subjected to uniformly distributed transverse loading

Li, Long-yuan

10.1080/15376494.2018.1432798
Mechanics of Advanced Materials and Structures
Taylor & Francis

MECHANICS OF ADVANCED MATERIALS AND STRUCTURES
https://doi.org/10.1080/15376494.2018.1432798
Received 10/09/2017
Accepted 15/11/2017

Effect of shear stress on distortional buckling of CFS beams subjected to uniformly distributed transverse loading

Jue Zhu[1] and Long-yuan Li[2]

(1) Faculty of Mechanical Engineering and Mechanics, Ningbo University, Ningbo 315211, China

(2) School of Engineering, University of Plymouth, Plymouth PL4 8AA, UK

Abstract – This paper presents an analytical investigation on the effects of shear stress and compressive stress gradient on the distortional buckling of cold-formed steel channel- and zed-section beams subjected to uniformly distributed transverse load. The study is performed by using the principle of minimum potential energy. It is shown that that for beams subjected to a uniformly distributed transverse load the buckling wave coupling in distortional buckling modes caused due to compressive stress gradient is very important, particularly for long beams. The effect of shear stress on the critical stress of distortional buckling exists but only in short beams. For beams longer than 3 m the shear stress effect can generally be ignored.

Keywords: Cold-formed steel, beams, distortional buckling, uniformly distributed load, shear stress.

1. Introduction

Thin-walled, cold-formed steel (CFS) sections have been widely used as the intermediate structural members in buildings for farming and industrial use. These sections, when subjected to compression and/or bending, may exhibit local, distortional, and lateral-torsional buckling. The types of local, distortional, and lateral-torsional buckling of a CFS member can

be distinguished by the shapes and half wavelengths of their buckling modes [1]. In general, the local buckling is a plate-like buckling of the compressed element in the section and has a relatively short half wavelength with the order of magnitude of the compressed element. The distortional buckling is similar to the local buckling of a stiffening element in a stiffened plate-like structure. For CFS channel- and zed-sections, this is usually represented by the rotation and translation of the compressed flange/lip about the web/flange junction. The half wavelength of the distortional buckling mode is generally several times greater than the largest characteristic dimension of the section. The lateral-torsional buckling of a CFS member may occur in two different ways. One is in the beams in which the tension flange is partially or fully restrained in its lateral direction; the other is in the beams in which there is no lateral or rotational restraint. The former is characterized by the translation and rotation of the free flange, which is in compression, with a distortion in the web; whereas the latter is considered to involve general lateral deflection and twist along the longitudinal direction of the member without any change in the cross-sectional shape. The half wavelength of the lateral-torsional buckling mode of a CFS member is similar to the beam length.

Unlike the local and lateral-torsional buckling of CFS members for which the critical loads can be calculated using the classical theories of plates and beams, the distortional buckling is a new type of buckling and it occurs mainly in CFS sections. The critical stress of the distortional buckling of a CFS member is dependent on not only the dimensions of the section but also the type of the applied load. Since Hancock's pioneered work [1] published in 1978, several approaches have been developed for determining the elastic critical stress of distortional buckling of CFS members. These include the analytical approaches, developed by Lau and Hancock [2] for CFS columns subjected to axial compression, Hancock [3], Li and Chen [4] for CFS beams subjected to bending, recommended in Eurocode 3 [5] for CFS

members subjected to compression and/or bending. In addition to the analytical models mentioned herein, numerical methods such as finite strip method [2, 6-11], finite element method [12-14], generalized beam theory (GBT) [15-18], neural network [19-21]) and experimental method [22-24] have also been used to analyse the distortional buckling of CFS columns and/or beams.

Note that in most methods mentioned above, the critical stress of distortional buckling is calculated only for members subjected to pure compression and/or pure bending. For CFS beams, however, the most common load is the distributed transverse load for which the pre-buckling stress in the beam varies not only within the cross-section, but also with the longitudinal axis of the beam. In literature, the variation of the pre-buckling stresses along the beam axis is often referred to as the moment gradient or stress gradient in order to distinguish it from the pure compression and/or pure bending that have no stress gradient along the longitudinal axis of the beam. A few of researchers have discussed the effect of stress gradient on the distortional buckling of CFS beams. For example, Chu et al. [7, 25] investigated the influence of stress gradient on the elastic distortional buckling stress of CFS channel- and zed-section beams using a semi-analytical method. Jiang and Davies [26] discussed the distortional buckling of restrained purlins under both downward and uplift loads using generalized beam theory. Chen and Li [27] proposed an analytical model by which the influence of stress gradient on the critical stress of distortional buckling was evaluated. Note that when there is a moment gradient in a beam, the pre-buckling stresses in the beam involve not only the axial tensile and compressive stresses but also the shear stresses. In literature, how the shear stress affects the critical stress of distortional buckling of a beam subjected to a uniformly distributed transverse load has not been discussed. In this paper, the influence of shear stress on the distortional buckling of CFS beams is investigated.

The analysis is performed by using the distortional buckling models proposed by Hancock [3], and Li and Chen [4]. The CFS sections investigated include channel- and zed-sections, which are the two most common types currently used in building constructions.

2. Overview of distortional buckling model

Consider a channel- or a zed-section beam with web depth h, flange width b, lip length c, and thickness t. Assume that the beam is subjected to a uniformly distributed transverse load, which causes the beam to be bent about its major axis. According to the distortional buckling model proposed by Li and Chen [4], the distortional buckling of CFS channel- and zed-sections can be represented by the combined torsional and flexural buckling of the compressed flange and lip system on elastic foundations as shown in Figure 1. The two elastic foundations are represented by two continuous springs; one is in horizontal direction (k_y) and the other is in vertical direction (k_z). The combined torsional and flexural buckling mode can be characterised by two independent displacements defined for the compressed flange/lip system. One is the translational displacement, $v(x)$, in the horizontal direction defined at the web/flange junction, and the other is the rotational displacement, $\phi(x)$, of the flange/lip system about the flange/web junction. The horizontal and vertical displacement components of the compressed flange/lip system at the shear centre (i.e. the flange/lip junction) and centroid point thus can be expressed as (v, $b\phi$) and (v-$z_o\phi$, (b-y_o)ϕ), respectively, where y_o and z_o are the horizontal and vertical distances between the centroid point and shear centre as indicated in Figure 1. The strain energy of the compressed flange and lip system under the buckling displacements $v(x)$ and $\phi(x)$ thus can be calculated in terms of the bending and twist of a thin-walled beam with an angle cross-section, expressed as follows,

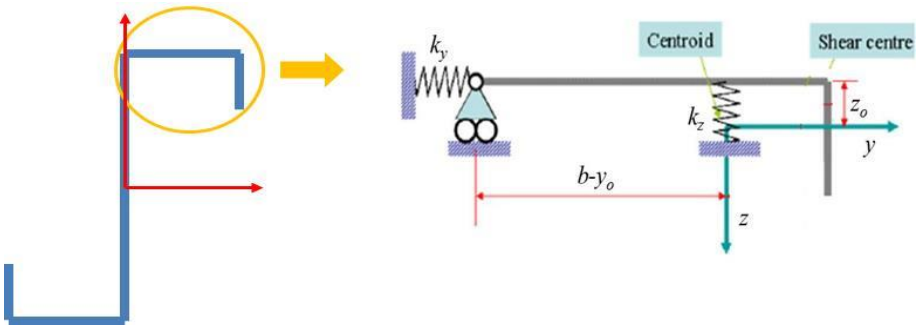

(a) (b)

Figure 1. (a) Zed-section. (b) Distortional buckling model for CFS channel- and zed-sections.

$$U = \frac{1}{2}\int_o^l \left[EI_y \left(\frac{d^2(b\phi)}{dx^2} \right)^2 + 2EI_{yz} \frac{d^2v}{dx^2} \frac{d^2(b\phi)}{dx^2} + EI_z \left(\frac{d^2v}{dx^2} \right)^2 \right] dx$$
$$+ \frac{1}{2}\int_o^l \left[EI_w \left(\frac{d^2\phi}{dx^2} \right)^2 + GJ \left(\frac{d\phi}{dx} \right)^2 \right] dx \qquad (1)$$
$$+ \frac{1}{2}\int_o^l \left[k_y v^2 + k_z (b - y_o)^2 \phi^2 \right] dx$$

where E is the Young's modulus, I_y and I_z are the second moments of area of the flange/lip system about y- and z-axes, I_{yz} is the product moment of area of the flange/lip system, I_w is the warping constant, G is the shear modulus, J is the torsion constant, k_y and k_z are the stiffnesses of the horizontal and vertical springs, and l is the beam length. The three integrations in Eq.(1) represents the strain energies of bending and twisting of the compressed flange/lip system, and the strain energy of the two springs, respectively.

Figure 2. Local coordinates and stress distribution in compressed flange/lip system.

The pre-buckling stresses of a channel- or a zed-section beam in the compressed flange/lip system involve both bending stress and shear stress (see Figure 2). Note that, for most channel- and zed-section beams the lip length, c, is much smaller than the section depth, h, and therefore the variation of bending stress in the lip can be ignored. The vertical displacement of the flange at a coordinate point η and the horizontal displacement of the lip at a coordinate point ζ can be expressed as $\eta\phi$ and v-$\zeta\phi$, respectively, which are needed for calculating the work done by the shear stresses, where η and ζ are the local coordinates defined in the flange and lip as indicated in Figure 2. The work done by the pre-buckling compressive and shear stresses in the flange/lip system thus can be calculated as follows,

$$W = \frac{A}{2}\int_o^l \sigma_b \left[\left(\frac{dv}{dx} - z_o \frac{d\phi}{dx} \right)^2 + \left((b - y_o) \frac{d\phi}{dx} \right)^2 + r_c^2 \left(\frac{d\phi}{dx} \right)^2 \right] dx + \frac{t}{2}\int_0^l \int_o^b 2\tau_{flange} \left(\frac{\partial(\eta\phi)}{\partial x} \right) \left(\frac{\partial(\eta\phi)}{\partial \eta} \right) dx d\eta + \frac{t}{2}\int_0^l \int_o^c 2\tau_{lip} \left(\frac{\partial(v - \zeta\phi)}{\partial x} \right) \left(\frac{\partial(v - \zeta\phi)}{\partial \zeta} \right) dx d\zeta \tag{2}$$

where $A = (b+c)t$ is the cross-sectional area of the flange/lip system, r_c is the polar radius of gyration of the flange/lip system with respect to its centroid, σ_b is the pre-buckling bending stress in the flange and lip, τ_{flange} and τ_{lip} are the pre-buckling shear stresses in the flange and lip, respectively, which, according to the bending theory of Bernoulli-Euler beams, can be expressed as follows,

$$\sigma_b = \sigma_{cr} \left(\frac{4x}{l} - \frac{4x^2}{l^2} \right) \tag{3}$$

$$\tau_{flange} = \frac{V(hc - c^2)}{2I_{zz}} + \frac{Vh(b - \eta)}{2I_{zz}} \tag{4}$$

$$\tau_{lip} = \frac{V(c - \zeta)}{I_{zz}} \left[\frac{h}{2} - \left(\zeta + \frac{c - \zeta}{2} \right) \right] \tag{5}$$

where σ_{cr} is the critical stress, V is the shear force, and I_{zz} is the second moment of area of the channel- or zed-section beam about zz-axis. For the case where the beam is subjected to a uniformly distributed load, the shear force can be expressed as follows,

$$V = \frac{q_{cr} l}{2}\left(1-\frac{2x}{l}\right) = \sigma_{cr}\frac{8I_{zz}}{hl}\left(1-\frac{2x}{l}\right) \tag{6}$$

where q_{cr} is the critical density of the uniformly distributed load. Substituting Eqs.(3)-(6) into (2), it yields,

$$\begin{aligned} W = {} & 2(b+c)t\sigma_{cr}\int_o^l\left(\frac{x}{l}-\frac{x^2}{l^2}\right)\left[\left(\frac{dv}{dx}-z_o\frac{d\phi}{dx}\right)^2+\left((b-y_o)^2+r_c^2\right)\left(\frac{d\phi}{dx}\right)^2\right]dx \\ & +\frac{2b^2t\sigma_{cr}}{l}\left(c-\frac{c^2}{h}+\frac{b}{3}\right)\int_0^l\left(1-\frac{2x}{l}\right)\phi\frac{d\phi}{dx}dx \\ & -\frac{2c^2t\sigma_{cr}}{l}\int_0^l\left(1-\frac{2x}{l}\right)\left[\left(1-\frac{4c}{3h}\right)v-c\left(\frac{1}{3}-\frac{c}{2h}\right)\phi\right]\frac{d\phi}{dx}dx \end{aligned} \tag{7}$$

where the first integration in Eq.(7) represents the work done by the axially compressive stress, whereas the second and third integrations represent the work done by the shear stresses, which represent the effect of shear stresses. The elastic critical stress σ_{cr} can be determined by using the following work-energy principle

$$\delta\Pi = \delta(U-W) = 0 \tag{8}$$

By assuming the displacement functions $v(x)$ and $\phi(x)$, one can solve the eigen-value of Eq.(8) and thus obtain the critical stress σ_{cr}. Note that, in general, $v(x)$ is much smaller than $c\phi(x)$, and thus can normally be ignored in the calculation [3,4]. For the simply supported beam, the rotation of the flange and lip system when it buckles can be assumed as

$$\phi(x) = \sum_{n=1} a_n \sin\frac{n\pi x}{l} \tag{9}$$

Substituting Eq.(9) and $v(x) = 0$ into (1) and (7) and noting that for any continuous function $f(x)$,

$$\int_o^l f(x)\phi(x)\frac{d\phi}{dx}dx=\left[f(x)\phi(x)\right]\phi(x)\Big|_o^l-\int_o^l\frac{d\left[f(x)\phi(x)\right]}{dx}\phi(x)dx$$
$$=-\int_o^l\frac{df(x)}{dx}\phi^2(x)dx-\int_o^l f(x)\frac{d\phi}{dx}\phi(x)dx=-\frac{1}{2}\int_o^l\frac{df(x)}{dx}\phi^2(x)dx \tag{10}$$

it yields,

$$U=\frac{l}{4}\sum_{n=1}\left[\left(EI_w+EI_yb^2\right)\left(\frac{n\pi}{l}\right)^4+GJ\left(\frac{n\pi}{l}\right)^2+k_z\left(b-y_o\right)^2\right]a_n^2 \tag{11}$$

$$W=\frac{\sigma_{cr}(b+c)t}{2l}\left[z_o^2+(b-y_o)^2+r_c^2\right]\left[\sum_{n=1}\left(\frac{n^2\pi^2}{3}-1\right)a_n^2-8\sum_{n=1}\sum_{m=1,m\neq n}\frac{mn(m^2+n^2)}{(m^2-n^2)^2}a_ma_n\right]$$
$$+\frac{\sigma_{cr}t}{l}\left[c^3\left(\frac{1}{3}-\frac{c}{2h}\right)+b^3\left(\frac{1}{3}+\frac{c}{b}-\frac{c^2}{hb}\right)\right]\sum_{n=1}a_n^2 \tag{12}$$

where the double series in the brackets in Eq.(12) contains only the terms, in which the sum (m+n) is an even number and m is not equal to n (see Page 109 in [28]). The two terms in Eq.(12) represents the work done by the axially compressive stress and shear stress, respectively. Substituting (11) and (12) into (8) and noting that for most CFS sections c/h <<1, it yields,

$$\left[\frac{\left(EI_w+EI_yb^2\right)}{(b+c)t}\left(\frac{n\pi}{l}\right)^4+\frac{GJ}{(b+c)t}\left(\frac{n\pi}{l}\right)^2+\frac{k_z\left(b-y_o\right)^2}{(b+c)t}\right]a_n$$
$$-\frac{2\sigma_{cr}\left(z_o^2+(b-y_o)^2+r_c^2\right)}{l^2}\times\left[\left(\frac{n^2\pi^2}{3}-1\right)a_n-8\sum_{m=1,m\neq n}\frac{nm(m^2+n^2)}{(m^2-n^2)^2}a_m\right] \tag{13}$$
$$-\frac{4\sigma_{cr}\left((b+c)^2-\frac{3bc^2}{b+c}\right)}{3l^2}\times a_n=0$$

Let,

$$\sigma_{cro}=\frac{\left(EI_w+EI_yb^2\right)\left(\frac{\pi}{\lambda_{cr}}\right)^2+GJ+k_z\left(b-y_o\right)^2\left(\frac{\lambda_{cr}}{\pi}\right)^2}{t\left(b+c\right)\left(z_o^2+(b-y_o)^2+r_c^2\right)} \tag{14}$$

$$k_{sh} = \frac{(b+c)^2 - \dfrac{3bc^2}{b+c}}{z_o^2 + (b - y_o)^2 + r_c^2} \tag{15}$$

where σ_{cro} is the critical stress of distortional buckling of the beam subjected to pure bending (i.e. there is no stress gradient in the pre-buckling stress) derived by Hancock [3], $\lambda_{cr} = l/n$ is the half wavelength of distortional buckling mode, and k_{sh} is a dimensionless factor, representing the effect of shear stresses in the flange and lip on distortional buckling. The spring constant k_z can be calculated as suggested in Refs. [3, 4, 27]. Hence, Eq.(13) can be simplified as follows,

$$\left[\frac{\sigma_{cro}}{\sigma_{cr}} - \frac{2}{3} + \frac{2}{(n\pi)^2}\left(1 - \frac{2k_{sh}}{3}\right)\right]a_n + \frac{16}{\pi^2}\sum_{m=1,m\neq n}\frac{m(m^2+n^2)}{n(m^2-n^2)^2}a_m = 0 \tag{16}$$

It is obvious from Eq.(16) that, if the work done by the shear stresses is ignored, that is $k_{sh} = 0$, then Eq.(16) reduces to the eigen-value equation derived by Chen and Li [27]. An examination of the shear effect factor for the sections with various different sizes produced by Albion Sections Ltd (see Table 1) indicates that k_{sh} is nearly equal to 3 (see Figure 3). Also, it is noted that for most channel- and zed-sections, λ_{cr} is about in the order of 500 mm [3-6, 27]. Thus, the largest value of n to be taken in Eq.(16) can be estimated according to the beam length. For instance, n should be at least 10 for a 5 m long beam. This indicates that the third term in the mid-bracket of Eq.(16) can be ignored for a long beam, implying that the effect of shear stresses on the critical stress of distortional buckling occurs only for short beams.

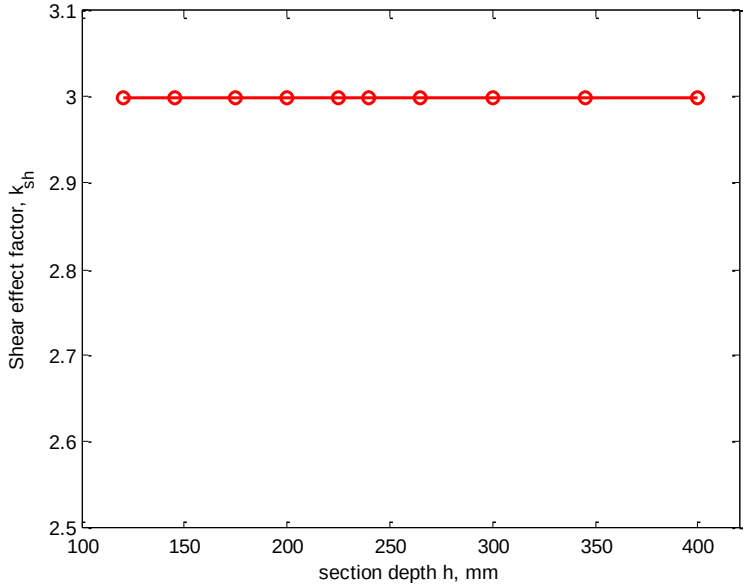

Figure 3. Shear effect factor for sections produced by Albion Sections Ltd.

3. Numerical examples

As numerical examples, four channel-section beams are considered herein, representing shallow, medium, deep and large-deep sections. Figures 4-7 shows the comparison of the critical stresses of distortional buckling calculated from Eq.(16), in which the red-colour lines are the results obtained by solving Eq.(16); the green-colour lines represent the results by solving Eq.(16) but ignoring the coupling terms of different wave numbers; the blue-colour lines represent the results by solving Eq.(16) but ignoring the shear stress effect. The results shown in Figures 4-7 demonstrate that the shear stress can significantly reduce the critical stress of distortional buckling but its effect is limited only for short beams. The comparison of the beams with different depths shows that, the deeper the beam section is, the larger the shear effect is. However, when the beam is greater than 4 m, the shear effect can generally be ignored. In contrast, the wave coupling is very important, particularly for beams greater than 1.5 m. The disregarding of wave coupling could significantly lead to an over-prediction of the

critical stress. The results shown in the figures also display that, with the increase of the beam length the critical stress of distortional buckling tends gradually to its lower limit, which is the critical stress of distortional buckling of the beam under pure bending.

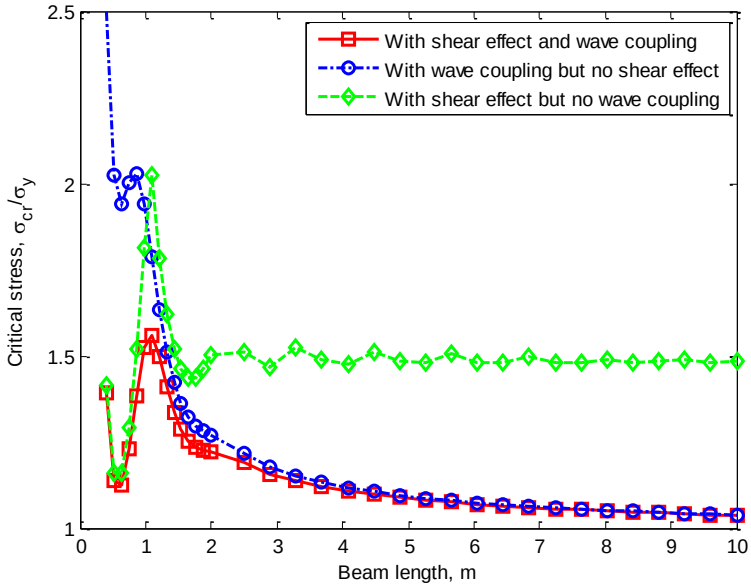

Figure 4. Comparison of critical stresses of distortional buckling of channel-section beam (h = 120 mm, b = 50 mm, c = 15 mm, t = 1.0 mm).

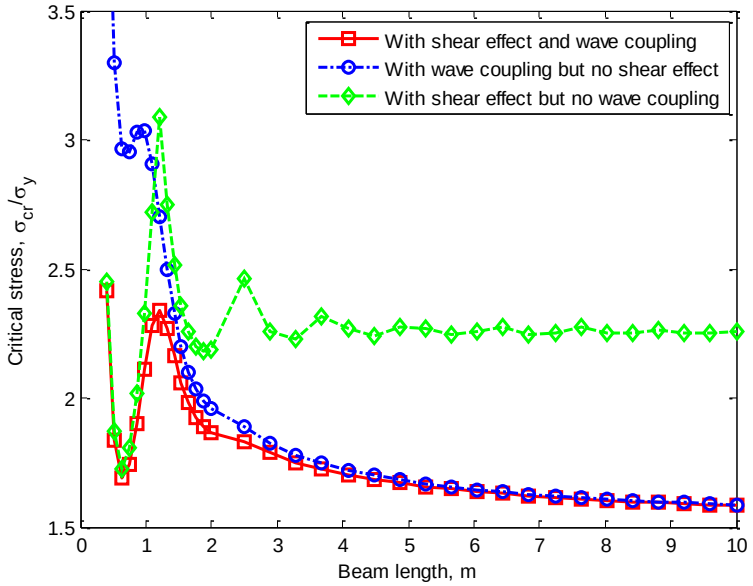

Figure 5. Comparison of critical stresses of distortional buckling of channel-section beam (h = 200 mm, b = 62.5 mm, c = 20 mm, t = 2.0 mm).

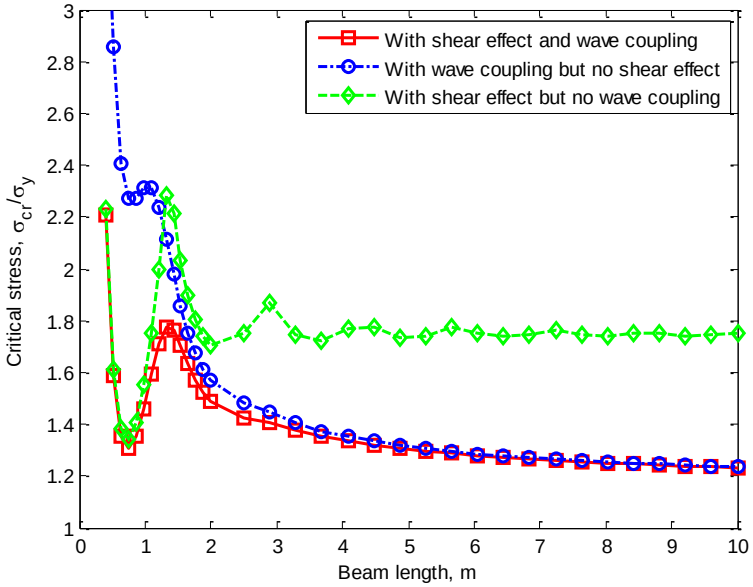

Figure 6. Comparison of critical stresses of distortional buckling of channel-section beam (h = 300 mm, b = 75 mm, c = 20 mm, t = 2.5 mm).

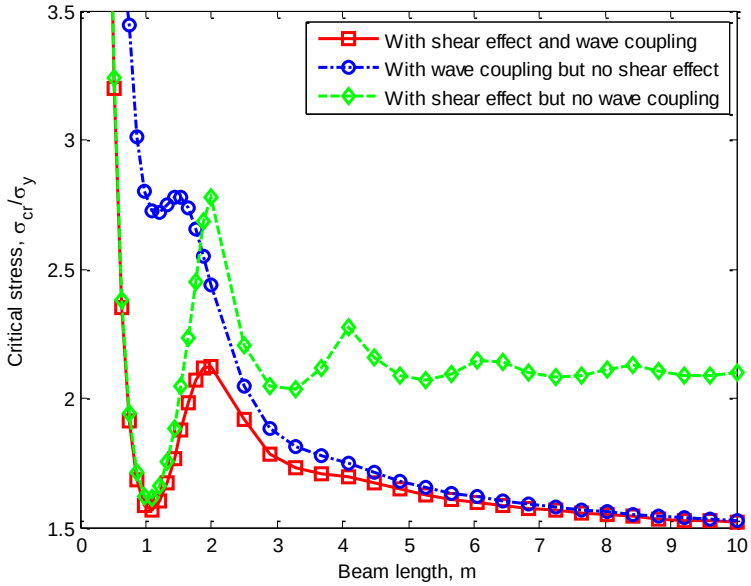

Figure 7. Comparison of critical stresses of distortional buckling of channel-section beam (h = 400 mm, b = 75 mm, c = 30 mm, t = 3.0 mm).

In order to demonstrate the present analytical model and the critical stress of distortional buckling calculated using Eq.(16), the finite element analyses of a channel-section beam of h = 200 mm, b = 70 mm, c = 20 mm, t = 2.5 mm with three different beam lengths (l = 500 mm, 1000 mm and 1500 mm) are also carried out using ANSYS software. The reason for selecting such a section size and such short beam lengths is to make sure the smaller critical stresses obtained from the finite element analysis include the distortional buckling mode [29]. The beam analysed is assumed to be simply supported at its two ends and subjected to a uniformly distributed transverse loads q_{cr} applied at the shear centre. In the finite element analyses the beam is modelled using 4-node thin shell elements. The simply supported boundary conditions are implemented by assuming all nodes at both end sections of the beam to have zero lateral displacement, zero transverse displacement, and zero rotational displacement about the longitudinal axis. To avoid the rigid displacement in the longitudinal direction of the beam a node located at the neutral plane at one of the end sections is assumed to have

zero axial displacement. The transverse distribution load is split into two parts, which are applied at the junctions between the web and two flanges. Because the shear centre of the channel section investigated here is away from the web line by 32 mm, a distribution twist moment generated due to eccentric distribution load is also applied at each loading line. The material properties of the beam are assumed as Young's modulus E = 205 GPa, Poisson ratio ν = 0.3, and yields stress σ_y = 390 MPa. The critical stress σ_{cr} is obtained by using eigen-buckling analysis. The corresponding ratios of critical stress to yield stress obtained from the finite element analyses are 1.77, 2.25 and 2.21, respectively; whereas those calculated from Eq.(16) are 1.98, 2.44 and 2.22. Overall, a good agreement is demonstrated. The largest difference between the two methods is 11.8%, which occurs in the beam with the length of 500 mm, which seems to be reasonable as the pre-buckling stress in the short beam does not follow the distribution described by the classical bending theory of Bernoulli-Euler beams.

4. Conclusions

This paper has presented an analytical investigation into the effect of shear stresses on the distortional buckling of simply supported CFS channel- and zed-section beams when they are subjected to uniformly distributed transverse loading. The study has been performed by using the distortional buckling models proposed by Hancock [3], Li and Chen [4] and Chen and Li 27]. From the present study the following conclusions can be drawn:

- The moment gradient in beams subjected to uniformly distributed transverse loading involves the axial compressive/tensile stress gradient and shear stress gradient. However, these two stress gradients have different effects on the distortional buckling of CFS zed- and channel-section beams.
- The axial compressive/tensile stress gradient can significantly alter the distortional buckling mode of the beam. It makes different wave terms be coupled, particularly for

long beams. Ignoring the wave coupling could significantly lead to an over-prediction of the critical stress.

- The shear stress gradient does not lead the wave coupling of the buckling modes. However, it can significantly reduce the critical stress of distortional buckling of short beams. For shallow- and medium-section beams longer than 2 m and for deep- and large deep-section beams longer than 4 m, the shear effect can generally be ignored.
- With the increase of the beam length, the critical stress of distortional buckling tends to its lower limit, which represents the critical stress of distortional buckling of the beam under pure bending.

Acknowledgements - The first author wishes to acknowledge the financial support received from National Natural Science Foundation of China (No.11572162), Natural Science Foundation of Zhejiang Province (No.LY13A020007), Ningbo Rail Transit of Ningbo City (JS-00-SG-17003), and K.C. Wong Magna Fund at Ningbo University for their financial support.

References

1. G.J. Hancock, Local, distortional and lateral buckling of I-beams, *Journal of Structural Division* (ASCE), vol. 104(11), pp. 1787-1798, 1978.
2. G.J. Hancock, Design for distortional buckling of flexural members, *Thin-Walled Structures*, vol. 27(1), pp. 3-12, 1997.
3. S.C.W. Lau, G.J. Hancock, Distortional buckling formulas for channel columns, *Journal of Structural Engineering* (ASCE), vol. 113(5), pp. 1063-1078, 1987.
4. L.Y. Li, J.K. Chen, An analytical model for analysing distortional buckling of cold-formed steel sections, *Thin-Walled Structures*, vol. 46(12), pp. 1430-1436, 2008.

5. EN1993-1-3, *Eurocode 3 - Design of Steel Structures - Part 1-3: General rules - Supplementary rules for cold-formed members and sheeting*, BSI, London, 2006.

6. S.C.W. Lau, G.J. Hancock, Buckling of thin flat-walled structures by a spline finite strip method, *Thin-Walled Structures*, vol. 4(4), pp. 269-294, 1986.

7. X.T. Chu, Z.M. Ye, R. Kettle, L.Y. Li, Buckling behaviour of cold-formed channel sections under uniformly distributed loads, *Thin-Walled Structures*, vol. 43(4), pp. 531-542, 2005.

8. S. Dong, H.R. Li, Q.P. Wen, Study on distortional buckling performance of cold-formed thin-walled steel flexural members with stiffeners in the flange, *Thin-Walled Structures*, vol. 95**,** pp. 161-169, 2015.

9. H.R. Naderian, H.R. Ronagh, M. Azhari, Elastic distortional buckling of doubly symmetric steel I-section beams with slender webs, *Thin-Walled Structures*, vol. 84, pp. 289-301, 2014.

10. B.W. Schafer, Z. Li, C.D. Moen, Computational modelling of cold-formed steel, *Thin-Walled Structures*, vol. 48(10–11), pp. 752-762, 2010.

11. Y.B. Yuan, S.S. Cheng, L.Y. Li, B. Kim, Web-flange distortional buckling of partially restrained cold-formed steel purlins under uplift loading, *International Journal of Mechanical Sciences*, vol. 89**,** pp. 476-481, 2014.

12. M. Casafont, F. Marimon, M.M. Pastor, Calculation of pure distortional elastic buckling loads of members subjected to compression via the finite element method, *Thin-Walled Structures*, vol. 47(6-7), pp. 701-729, 2009.

13. M.R. Haidarali, N.A. Nethercot, Local and distortional buckling of cold-formed steel beams with both edge and intermediate stiffeners in their compression flanges, *Thin-Walled Structures*, vol. 54, pp. 106-112, 2012.

14. S. Niu, K.J.R. Rasmussen, F. Fan, Distortional–global interaction buckling of stainless steel C-beams: Part II-Numerical study and design, *Journal of Constructional Steel Research*, vol. 96, pp. 40-53, 2014.

15. J.M. Davis, P. Leach, First-order generalized beam theory, *Journal of Constructional Steel Research*, vol. 31(2/3), pp. 187-220, 1994.

16. J.M. Davis, P. Leach, Second-order generalized beam theory, *Journal of Constructional Steel Research*, vol. 31(2/3), pp. 221-241, 1994.

17. R. Schardt, Lateral torsional and distortional buckling of channel- and hat-sections, *Journal of Constructional Steel Research*, vol. 31(2-3), pp. 243-265, 1994.

18. N. Silvestre, D. Camotim, Distortional buckling formulae for cold-formed steel c- and z-section members, Part I - derivation, *Thin-Walled Structures*, vol. 42(11), pp. 1599-1629, 2004.

19. M. Pala, A new formulation for distortional buckling stress in cold-formed steel members, *Journal of Constructional Steel Research*, vol. 62(7), pp. 716-722, 2006.

20. M. Pala, Genetic programming-based formulation for distortional buckling stress of cold-formed steel members, *Journal of Constructional Steel Research*, vol. 64(12), pp. 1495-1504, 2008.

21. M. Pala, N. Caglar, A parametric study for distortional buckling stress on cold-formed steel using a neural network, *Journal of Constructional Steel Research*, vol. 63(5), pp. 686-691, 2007.

22. M. Casafont, M.M. Pastor, F. Roure, T. Peköz, An experimental investigation of distortional buckling of steel storage rack columns, *Thin-Walled Structures*, vol. 49(8), pp. 933-946, 2011.

23. E.S. dos Santos, E.M. Batista, D. Camotim, Experimental investigation concerning lipped channel columns undergoing local–distortional–global buckling mode interaction, *Thin-Walled Structures*, vol. 54, pp. 19-34, 2012.

24. S. Niu, K.J.R. Rasmussen, F. Fan, Distortional-global interaction buckling of stainless steel C-beams: Part I - Experimental investigation, *Journal of Constructional Steel Research*, vol. 96, pp. 127-139, 2014.

25. X.T. Chu, Z.M. Ye, L.Y. Li, R. Kettle, Local and distortional buckling of cold-formed zed-section beams under uniformly distributed transverse loads, *International Journal of Mechanical Sciences*, vol. 48(4), pp. 378-388, 2006.

26. C. Jiang, M.J. Davies, Design of thin-walled purlins for distortional buckling, *Thin-Walled Structures*, vol. 29(1-4), pp. 189-202, 1997.

27. J.K. Chen, L.Y. Li, Distortional buckling of cold-formed steel sections subjected to uniformly distributed transverse loading, *International Journal of Structural Stability and Dynamics*, vol. 10(5), pp. 1017-1030, 2010.

28. S.P. Timoshenko, J.M. Gere, *Theory of Elastic Stability*, McGraw Hill, New York, 1961.

29. W.B. Yuan, N.T. Yu, L.Y. Li, Distortional buckling of perforated cold-formed steel channel-section beams with circular holes in web, *International Journal of Mechanical Sciences*, vol. 126, pp. 255-260, 2017.

Table 1: Dimensions of CFS channel-sections produced by Albion Sections (unit: mm)

Sections	Web depth, *h*	Flange width, *b*	Lip length, *c*	Thickness, *t*
C12515	120	50	15	1.5
C12516	120	50	15	1.6
C14613	145	62.5	20	1.3
C14614	145	62.5	20	1.4
C14615	145	62.5	20	1.5
C14616	145	62.5	20	1.6

C14618	145	62.5	20	1.8
C14620	145	62.5	20	2.0
C17613	175	62.5	20	1.3
C17614	175	62.5	20	1.4
C17615	175	62.5	20	1.5
C17616	175	62.5	20	1.6
C17618	175	62.5	20	1.8
C17620	175	62.5	20	2.0
C17623	175	62.5	20	2.3
C17625	175	62.5	20	2.5
C20613	200	65	20	1.3
C20614	200	65	20	1.4
C20615	200	65	20	1.5
C20616	200	65	20	1.6
C20618	200	65	20	1.8
C20620	200	65	20	2.0
C20623	200	65	20	2.3
C20625	200	65	20	2.5
C22614	225	65	20	1.4
C22615	225	65	20	1.5
C22616	225	65	20	1.6
C22618	225	65	20	1.8
C22620	225	65	20	2.0
C22623	225	65	20	2.3
C22625	225	65	20	2.5
C24615	240	65	20	1.5
C24616	240	65	20	1.6
C24618	240	65	20	1.8
C24620	240	65	20	2.0
C24623	240	65	20	2.3
C24625	240	65	20	2.5
C24630	240	65	20	3.0
C26616	265	65	20	1.6
C26618	265	65	20	1.8
C26620	265	65	20	2.0
C26623	265	65	20	2.3
C26625	265	65	20	2.5
C26630	265	65	20	3.0
C30718	300	75	20	1.8
C30720	300	75	20	2.0
C30723	300	75	20	2.3
C30725	300	75	20	2.5
C30730	300	75	20	3.0
C34118	345	100	30	1.8
C34120	345	100	30	2.0
C34123	345	100	30	2.3
C34125	345	100	30	2.5
C34130	345	100	30	3.0

C40120	400	100	30	2.0
C40123	400	100	30	2.3
C40125	400	100	30	2.5
C40130	400	100	30	3.0
C40132	400	100	30	3.2